Available online at www.sciencedirect.com
SCIENCE DIRECT®
Journal of Sound and Vibration 266 (2003) 281–305
JOURNAL OF SOUND AND VIBRATION
www.elsevier.com/locate/jsvi

Elastic wave scattering around cavities in inhomogeneous continua by the BEM

G.D. Manolis*

Department of Civil Engineering, School of Engineering, P.O. Box 502, Aristotle University, Thessaloniki, GR-54124, Greece

Received 30 April 2002; accepted 11 September 2002

Abstract

This work examines elastic wave scattering around cavities embedded in a continuum with depth-dependent shear modulus and under conditions of plane strain. A restricted case of inhomogeneity is considered, where the Poisson ratio is fixed at 0.25 and where the density profile also varies, but proportionally to the shear modulus. For this specific case, the wave speeds remain macroscopically constant and it becomes possible to recover the exact Green functions by using an algebraic transformation method. These functions are subsequently used as kernels in a standard 2D boundary element formulation defined in the Laplace transform domain. The final step involves an inverse Laplace transformation, whereby the transient behavior of cavities in the aforementioned inhomogeneous continuum can be recovered. Two basic examples are solved, namely the circular cylindrical cavity under sudden internal explosion and under a pressure wave sweep. In the latter case, it is possible to investigate the effect that the angle of wave incidence has on the displacement and stress that develop along the cavity's perimeter, given the fact that the shear modulus is changing along the vertical direction. These examples serve to illustrate the present approach and to reveal some interesting differences that are observed in transient wave scattering phenomena between homogeneous and continuously inhomogeneous models, where the latter models yield a more realistic representation of geological formations.

1. Introduction

Wave motion in naturally occurring formations as well as in man-made materials is a subject under continuous investigation [1–4] because of widespread applications in a number of scientific fields; acoustic and electromagnetic signal transmissions, seismically induced ground motions, subsurface exploration, non-destructive testing evaluation and mechanical properties of materials,

*Tel.: +3-2310-995-663; fax: +3-2310-995-769.
E-mail address: gdm@civil.auth.gr (G.D. Manolis).

0022-460X/03/$ - see front matter
doi:10.1016/S0022-460X(03)00175-5

noise pollution control, deep water acoustics, etc., are all governed by scalar or vector wave equations. Due to the complex structure of such media, wave propagation is invariably accompanied by reflection, refraction, diffraction and scattering phenomena that are difficult to quantify. As a result, it becomes necessary to introduce a number of refinements in the standard mathematical description of these problems such as position-dependent moduli, layering, anisotropy, etc., [5,6]. Additional phenomena that may have to be accounted for are structural periodicity [7], damping mechanisms [8], material parameter fluctuations [9], the presence of cracks [10] and the existence of a second phase within the original material [11]. In general, the complexity of all these classes of problems is such that most cases must be examined individually and within the context of specific applications. Furthermore, recourse to specialized numerical methods of solution, such as boundary integral equations, is often an imperative [12,13].

Elastic waves in discretely layered media and in variable velocity layers are discussed in Ewing et al. [1], where the basic problem of inseparability of waves into dilatational and rotational components is brought forth. Brekhovskikh and Beyer [14] and Chew [15] examine primarily acoustic and electromagnetic waves, with the former reference focusing on wave reflection and refraction in discrete as well as in continuously layered media and the latter on specialized methods such as variational techniques, mode matching, the Green functions, integral equations and the T-matrix approach which can be used for numerical solution of problems involving waves in planar, cylindrically and spherically layered media. In general, most of the work on waves in inhomogeneous continua focuses on acoustic and electromagnetic waves in discretely layered media and under time-harmonic conditions. Of major importance is the planar scalar wave equation with a depth-dependent wave number, because it corresponds to (a) sound waves when acoustic medium density variation over the wavelength is negligible, (b) electromagnetic waves when the electric field is polarized and (c) horizontally as well as vertically polarized elastic shear waves. In this latter case, it is necessary to resort to a potential representation of the displacement vector in order to recover two scalar wave equations, so that certain restrictions on the medium inhomogeneity need to be imposed. Furthermore, the problems most often considered are wave reflection and refraction at an interface separating two media, while wave scattering problems in most cases require numerical techniques for their solution.

Wave motion in geological media presents certain peculiarities that have to do with the inherent difficulty of providing an accurate description of the underlying soil and rock formations [5,16]. As a result, many specialized methods for analyzing seismically induced ground motions have been devised [17]. For instance, Geller and Ohminato [18] compute synthetic seismograms for laterally and vertically heterogeneous media, consisting of both solid and fluid regions, by the direct solution method. Specifically, their formulation derives from the addition of appropriate surface integrals to the weak (Galerkin) form of the governing equations of motion followed by enforcement of all the necessary boundary conditions. A hybrid method for computing seismic motion in non-homogeneous viscoelastic topography is presented in Moczo et al. [19] by combining the discrete wavenumber method with finite differences and with finite elements, while a specialized finite element approach was used by Kim et al. [20] for simulating the cross-hole experimental procedure, which is used to determine material properties of in situ soil deposits as well as their variation with depth. Gragg [21] analyzed 1-D wave motion in a weakly non-uniform medium by recasting the governing Helmholtz equation as a first order, initial-value problem and employing d'Alembert's decomposition. By assuming negligible signal backscattering, a solution

is derived whereby the forward and backward travelling waves generated at a discontinuity are uncoupled, their separate energies are conserved and coupling has a residual effect on their phases only. Muravskii [22] studied time-harmonic surface waves in a linearly inhomogeneous half-space, where Rayleigh and Lamb waves are manifested at large distances form the point of application of vertical and horizontal forces, respectively. By quantifying the manner in which medium inhomogeneity affects the complex amplitude and frequency contents of the ensuing vibrations, it is possible to tabulate information from which the shear modulus variation and energy dissipation characteristics of the material in question can be deduced from experimental measurements. Finally, numerical approaches such as those mentioned above find application in structural mechanics as well. For instance, Volovoi et al. [23] compute dispersion curves for beams with non-prismatic cross-section made from non-homogeneous, anisotropic materials by using finite element analysis based on higher order beam theory.

An alternative approach for modelling geological media is to assume that inhomogeneities are randomly distributed across a homogeneous background and then use stochastic methods of analysis [24]. There are also efforts towards obtaining effective properties plus their bounds for various types of heterogeneous materials (such as composites) by considering families of specimens of different sizes for the material in question and then using stochastic averaging techniques [25].

In this work, one focuses on the dynamic response of underground openings in an inhomogeneous continuum where both shear modulus and density vary proportionally in the vertical direction, so that the wave speeds of the travelling pressure (P) and shear (S) waves are macroscopically constant. A direct boundary integral equation formulation defined in the Laplace transform (LT) domain is employed, and time dependence of the resulting displacements, tractions and stresses is recovered through the inverse transformation. Numerical implementation of the aforementioned formulation is of the boundary element method (BEM) type, whose power in solving dynamic problems for continuous media has been amply demonstrated over the past 20 years or so [26,27]. There are two basic avenues for extending the BEM to the various cases that arise when time-dependent behavior of natural media or manufactured materials is sought: (a) use of specialized fundamental solutions or the Green functions [28] so that the chief advantage of the BEM, namely surface discretization only, is preserved and (b) use of volume discretization by converting the difference between the actual mechanical state and a basic state that corresponds to ideal linear elastic, homogeneous and isotropic conditions into a body force. This is known as the dual-reciprocity BEM [29]. The resulting volume integral is subsequently computed with the help of specialized functions so that relatively few interior nodes are required for maintaining good numerical accuracy.

For non-homogeneous isotropic materials, Chen et al. [30] developed a generalized BEM where the domain integral involves first order derivatives of the displacement kernel. By using radial basis functions, the domain integral is converted into a boundary integral so that numerical implementation for 2-D elastostatics is performed using a surface mesh plus relatively few internal collocation points. Also, Itagaki [31] developed a dual-reciprocity BEM for Helmholtz-type equations with a space-dependent source term based on repeated application of particular solutions for the Poisson equation. This scheme was subsequently expanded to iteratively solve problems involving non-uniform media. Similarly, Xu and Kamiya [32] approximated the inhomogeneous term for non-linear potential problems by polynomials whose coefficients were

determined in a least-square sense from a system of integral equations defined at both boundary and interior domain of the problem in question.

Analytical solutions for the steady state response of layered acoustic as well as elastic formations that are valid at high frequencies and can serve as the Green functions for a BEM analysis of 3-D fluid–structure interaction problems appear in Tadeu and Antonio [33]. An efficient method based on the Hankel transform combined with matrix formalism was recently derived by Wang and Ishikawa [34] for computing displacements and stresses in multilayered media under axisymmetric conditions. Furthermore, boundary integral equation formulations for the solution of static deformations in continuously inhomogeneous, anisotropic solids have also appeared recently through the introduction of appropriate kernel functions [35]. Finally, among other recent work on the computation of the specialized Green functions one mentions that of Guzina and Pak [36] on the response of a vertically heterogeneous elastic half-space with smooth modulus variation under a set of time-harmonic ring and point sources via asymptotic decomposition of the displacement vector, and that of Vrettos [37] on the response of a compressible and continuously non-homogeneous elastic soil to a static vertical load at the surface by using classical integral transform techniques and the extended power series method.

In sum, the present BEM approach employs the specialized Green functions that are exact solutions to the boundary-value problem of a point force in a continuously inhomogeneous 2-D elastic medium whose precise description was given above. These Green functions are derived following the method originally developed for a 3-D continuum in Manolis and Shaw [38]. They are subsequently used as kernel functions within the context of a standard BEM program and a series of numerical example are solved involving underground openings so as to demonstrate the efficiency of the present approach and to help draw conclusions on the vibration characteristics of these openings as they are swept by elastic waves.

2. Governing equations of motion

The dynamic equilibrium equations, the kinematic relations and the constitutive law for a linear elastic, isotropic medium are

$$\sigma_{ij,j} + \rho f_i = \rho \ddot{u}_i, \qquad \varepsilon_{ij} = 0.5(u_{i,j} + u_{j,i}), \qquad \sigma_{ij} = \lambda\theta\delta_{ij} + 2\mu\varepsilon_{ij}. \tag{1}$$

In the above, u_i, ρf_i, ε_{ij} and σ_{ij}, respectively, are the displacements, the body forces per unit volume, the strains and the stresses, while λ, μ are the Lamé constants and ρ is the mass density. Furthermore, $\theta = \varepsilon_{kk} = u_{k,k}$ is the dilatation. All indices range from 1 to 2 in 2-D, with commas indicating partial differentiation with respect to the spatial co-ordinates x_i and dots indicating partial derivatives with respect to time t. Finally, the summation convention is implied for repeated indices and δ_{ij} is Kronecker's delta.

In the case of a homogeneous medium, Eqs. (1) combine to give the well-known Navier–Cauchy equations that govern elastic wave propagation as

$$(\lambda + \mu)u_{j,ji} + \mu u_{i,jj} + \rho f_i = \rho \ddot{u}_i. \tag{2}$$

In vector form, these equations are

$$(\lambda+\mu)\nabla\nabla\bullet\mathbf{u}+\mu\nabla^2\mathbf{u}+\rho\boldsymbol{f}=\rho\ddot{\mathbf{u}} \tag{3}$$

where ∇ is the gradient and ∇^2 is the Laplacian. If the continuum is heterogeneous, then the material parameters are position dependent (e.g., $\lambda=\lambda(\mathbf{x})$, $\mu=\mu(\mathbf{x})$, $\rho=\rho(\mathbf{x})$) and the Navier–Cauchy equations are recovered in a form different from that shown above. More specifically, a first step yields

$$\{\lambda(\mathbf{x})u_{k,k}(\mathbf{x},t)\}_{,i}+\{\mu(\mathbf{x})(u_{i,j}(\mathbf{x},t)+u_{j,i}(\mathbf{x},t))\}_{,j}+\rho(\mathbf{x})f_i(\mathbf{x},t)=\rho(\mathbf{x})\ddot{u}_i(\mathbf{x},t). \tag{4}$$

Once the differentiations have been carried out we have, in vector form, that

$$\nabla\{(\lambda+2\mu)\theta\}+\mu\nabla^2\mathbf{u}-\mu\nabla\theta-2\theta\nabla\mu+2\nabla\mu\cdot\mathbf{E}+\rho\mathbf{f}=\rho\ddot{\mathbf{u}} \tag{5}$$

where $\mathbf{E}$ is the strain tensor ε_{ij}. The above equation appears in Ewing et al. [1], where it is mentioned that unless the variation of the material parameters over a wavelength is small, there is coupling between pressure and shear waves at every point of the continuum. Therefore, an approach based on the Helmholtz vector decomposition will not work.

2.1. Algebraic transformation procedure

In order to obtain a fundamental solution for the dynamic equilibrium equations governing elastic wave propagation in a restricted class of heterogeneous continua, the following algebraic transformation that was originally established for 3-D cases [38] is employed here in conjunction with the displacement vector $\mathbf{u}=(u_1, u_2)$ as

$$\mathbf{u}(\mathbf{x},t)=T(\mathbf{x})\mathbf{U}(\mathbf{x},t), \tag{6}$$

$$T(\mathbf{x})=\mu^{-1/2}(\mathbf{x}). \tag{7}$$

Using this transformation, a quadratic profile for the shear modulus with respect to the depth $x_2=y$ co-ordinate is recovered as

$$\mu(y)=(ay+b)^2, \tag{8}$$

where a, b are constants. By taking all the resulting constraints into account [38], the final form of the dynamic equilibrium equations is

$$\mu(y)U_{i,jj}+2\mu(y)U_{j,ij}+\rho(y)\mu^{1/2}(y)f_i=\rho(y)\ddot{U}_i. \tag{9}$$

One notes here that $T(\mathbf{x})$ belongs to the group of "reverse" transformations in the sense that the material profiles for which it is applicable are recovered a posteriori as constraint functions. Thus, it is not as general as integral-type transforms, but instead has the advantage that it is simple to invert, i.e., $\mathbf{U}=T^{-1/2}\mathbf{u}$. If the same transformation is used for the body force so that $f_i(\mathbf{x},t)=\mu^{-1/2}(y)F_i(\mathbf{x},t)$, then

$$U_{i,jj}+2U_{j,ij}+\rho(y)F_i=(\rho(y)/\mu(y))\ddot{U}_i. \tag{10}$$

3. The LT domain solution

The LT with respect to the time variable of a given function $f(t)$ and the inverse transformation are defined as [39]

$$\tilde{f}(s) = \int_0^\infty f(t)\exp(-st)\,\mathrm{d}t, \quad \mathrm{Re}\{s\} > 0,$$

$$f(t) = \frac{1}{2\pi \mathrm{i}}\int_{c-\infty}^{c+\mathrm{i}\infty} \tilde{f}(s)\exp(st)\,\mathrm{d}t, \quad 0 < t < \infty, \tag{11}$$

where c is greater than the real part of all singularities of $\tilde{f}(s)$. The LT of the previous equation of motion (10) with zero initial conditions becomes

$$\tilde{U}_{i,jj} + 2\tilde{U}_{j,ij} - s^2(\rho(y)/\mu(y))\tilde{U}_i = -\rho(y)\tilde{F}_i. \tag{12}$$

If the original forcing function is assumed to be a point impulse in time, i.e., $f_i(\mathbf{x}, t) = f_0\delta(\mathbf{x})\delta(t)$, and if the shear modulus and density variations remain proportional as $\rho(y)/\mu(y) = \rho_0/\mu_0$, then

$$\tilde{U}_{i,jj} + 2\tilde{U}_{j,ij} - s^2(\rho_0/\mu_0)\tilde{U}_i = -\rho(y)f_0\delta(\mathbf{x}) = -\rho_0 f_0\delta(\mathbf{x}) \tag{13}$$

In the above, ρ_0, μ_0 are the values of the material parameters at the point of application of the load, which is labelled as the source and assumed to be at the origin of the co-ordinate system ($\mathbf{x} = 0$). Eq. (13) is equivalent to the transformed equation of motion of a homogeneous solid. Thus, its solution can be recovered by standard methods of elastodynamics, such as the use of potentials, the dynamic equivalent to Galerkin's vector, etc. [2,3].

3.1. Displacement fundamental solution

The procedure by which the Green function can be recovered for a dynamic equilibrium equation such as Eq. (13) follows Cruse and Rizzo [40], i.e.,

$$\tilde{G}_{ij} = (f_0/2\pi\mu_0)[\psi\delta_{ij} - \chi r_{,i}r_{ij}], \tag{14}$$

where

$$\psi = \mathrm{K}_0(sr/c_2) + (c_2/sr)[\mathrm{K}_1(sr/c_2) - (c_2/c_1)\mathrm{K}_1(sr/c_1)],$$

$$\chi = \mathrm{K}_2(sr/c_2) - (c_2^2/c_1^2)\mathrm{K}_2(sr/c_1). \tag{15}$$

As shown in Fig. 1(a), imposition of a unit point force at source $\boldsymbol{\xi}$ in both directions produces the displacement components $\tilde{G}_{ij}$ at receiver $\mathbf{x}$, which is at a distance r away. Furthermore, K_m are the modified Bessel functions of second kind and order m, while s is the LT parameter and c_1, c_2 are the P- and S-wave speeds. One notes in passing that for zero initial conditions, the Laplace transform results are equivalent to Fourier transformed results if $s = \mathrm{i}\omega$, where ω is the frequency parameter and $\mathrm{i} = \sqrt{-1}$. Also, because the delta function is defined only at $\boldsymbol{\xi}$, the relevant value of the shear modulus is that registered at the source, i.e., $\mu = \mu(\boldsymbol{\xi}) = \mu_0$. Finally, the wave speeds appearing above are macroscopically constant since for the particular type of inhomogeneity examined herein, both shear modulus and density vary proportionally. Thus, $c_2^2 = \mu(\mathbf{x})/\rho(\mathbf{x}) = \mu_0/\rho_0$ and $c_1 = \sqrt{3}c_2$ for the Poisson ratio of $v = 0.25$.

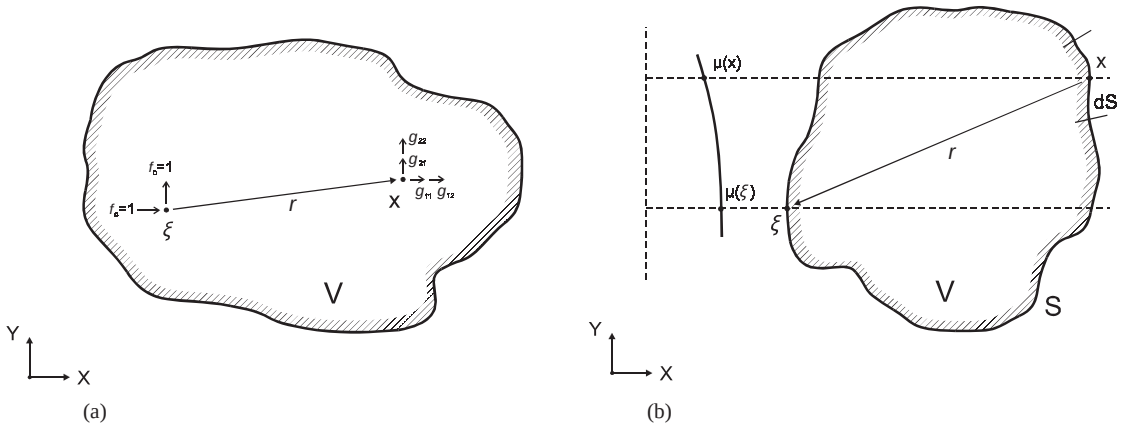

Fig. 1. Definitions for (a) the displacement fundamental solution and (b) the surface discretization of the inhomogenous solid.

The next step is to perform the inverse of the algebraic transformation defined by Eq. (6) so as to recover the Green function $\tilde{g}_{ij}(\mathbf{x},\boldsymbol{\xi})$ in the original domain. Specifically, the inverse transformation yields

$$\tilde{g}_{ij} = \mu^{-1/2}(\mathbf{x})\tilde{G}_{ij} = \mu^{-1/2}(\mathbf{x})\mu^{-1/2}(\boldsymbol{\xi})[f_0/2\pi][\psi\delta_{ij} - \chi r_{,i}\, r_{,j}]. \tag{16}$$

3.2. Traction fundamental solution

The $\tilde{f}_{ij}$ kernel is derived for $\tilde{g}_{ij}(\mathbf{x},\boldsymbol{\xi})$ by using first principles. Specifically, the displacements u_i and the tractions t_i are defined as

$$u_i = g_{ij}e_j, \qquad t_i = \sigma_{ij}n_j, \qquad t_i = f_{ij}e_j. \tag{17}$$

where e_j and n_j are the unit vector and the outward pointing normal vector, respectively, while the kinematic relations and the constitutive law appearing in Eq. (1) are still relevant. The operations indicated in Eqs. (1) and (17) are done with respect to field point $\mathbf{x}$, which implies that the value of the shear modulus at $\boldsymbol{\xi}$ remains fixed as f_{ij} is being computed. Also, the $(\sim)$ superscript, which indicates LT values, is dropped for notational convenience.

In view of Eq. (17), plus the fact that $\lambda = \mu$ for our particular type of inhomogeneity, the stresses are given as

$$\begin{aligned}
\sigma_{11} &= \mu(x_2)[3g_{11,1}e_1 + 3g_{12,1}e_2 + g_{21,2}e_1 + g_{22,2}e_2],\\
\sigma_{22} &= \mu(x_2)[g_{11,1}e_1 + g_{12,1}e_2 + 3g_{21,2}e_1 + 3g_{22,2}e_2],\\
\sigma_{12} &= \mu(x_2)[g_{11,2}e_1 + g_{12,2}e_2 + g_{21,1}e_1 + g_{22,1}e_2] = \sigma_{21},
\end{aligned} \tag{18}$$

where x_2 is the vertical co-ordinate of field point $\mathbf{x}$.

Next, the tractions t_i are grouped using matrix notation as

$$\begin{Bmatrix} t_1 \\ t_2 \end{Bmatrix} = \left[\begin{array}{c|c} f_{11} & f_{12} \\ f_{21} & f_{22} \end{array}\right] \begin{Bmatrix} e_1 \\ e_2 \end{Bmatrix} = \mu(x_2) \times \left[\begin{array}{c|c} (3g_{11,1}+g_{21,2})n_1+(g_{11,2}+g_{21,1})n_2 & (3g_{12,1}+g_{22,2})n_1+(g_{12,2}+g_{22,1})n_2 \\ (g_{11,1}+g_{21,1})n_1+(g_{11,1}+3g_{21,2})n_2 & (g_{12,2}+g_{22,1})n_1+(g_{12,1}+3g_{22,2})n_2 \end{array}\right] \begin{Bmatrix} e_1 \\ e_2 \end{Bmatrix}. \quad (19)$$

Based on the above expansion, the traction kernel can be written in compact form as

$$f_{ij}(\mathbf{x},\boldsymbol{\xi}) = \mu^{-1/2}(x_2)\hat{f}_{ij}\mu^{-1/2}(\xi_2) + \mathbf{D}_{(x)}[\mu^{-1/2}(x_2)]\hat{g}_{ij}\mu^{-1/2}(\boldsymbol{\xi}_2) = f_{ij}^{(1)} + f_{ij}^{(2)}. \quad (20)$$

The $\hat{f}_{ij}$ and $\hat{g}_{ij}$ parts correspond to the homogeneous medium solutions [40] divided by the shear modulus μ, namely

$$\hat{g}_{ij} = \frac{(f_0=1)}{2\pi}[\psi\delta_{ij} - \chi r_{,i}\, r_{,j}] \quad (21)$$

and

$$\hat{f}_{ij} = \frac{1}{2\pi\mu}\left[\left(\frac{\mathrm{d}\psi}{\mathrm{d}r} - \frac{1}{r}\chi\right)\left(\delta_{ij}\frac{\partial r}{\partial n} + r_{,j}\, n_i\right) - \frac{2}{r}\chi\left(n_j r_{,i} - 2r_{,i}\, r_{,j}\frac{\partial r}{\partial n}\right) - 2\frac{\mathrm{d}\chi}{\mathrm{d}r} r_{,i}\, r_{,j}\frac{\partial r}{\partial n} + \left(\frac{c_1^2}{c_2^2} - 2\right)\left(\frac{\mathrm{d}\psi}{\mathrm{d}r} - \frac{\mathrm{d}\chi}{\mathrm{d}r} - \frac{\chi}{r}\right) r_{,i}\, n_j\right]. \quad (22)$$

In the latter case, μ is the value at $\mathbf{x}$ and

$$r\frac{\mathrm{d}\psi}{\mathrm{d}r} = -[sr/c_2 + 2c_2/sr]K_1(sr/c_2) + [2c_2^2/c_1 sr]K_1(sr/c_1) - K_0(sr/c_2) + [c_2^2/c_1^2]K_0(sr/c_1),$$

$$r\frac{\mathrm{d}x}{\mathrm{d}r} = -[sr/c_2 + 4c_2/sr]K_1(sr/c_2) + (c_2^2/c_1^2)[sr/c_1 + 4c_1/sr]K_1(sr/c_1) - 2K_0(sr/c_2) + [2c_2^2/c_1^2]K_0(sr/c_1). \quad (23)$$

The operator $\mathbf{D}_{(\mathbf{x})}$ is simply the derivative with respect to the vertical direction at $\mathbf{x}$. Thus, if $\mu(x_2) = (ax_2 + b)^2$, then

$$\partial[\mu^{-1/2}(x_2)]/\partial x_1 = 0, \qquad \partial[\mu^{-1/2}(x_2)]/\partial x_2 = -a/\mu(x_2). \quad (24)$$

Given the specific profile of μ, constants $a = (\sqrt{\mu_1} - \sqrt{\mu_0})/L$ and $b = \sqrt{\mu_0}$, where L is the vertical distance separating points $\mathbf{x}$ and $\boldsymbol{\xi}$.

Carrying out the algebra, Eq. (20) attains the final form

$$f_{ij}(\boldsymbol{x},\boldsymbol{\xi}) = \mu^{1/2}(x_2)\bar{f}_{ij}(r)\mu^{-1/2}(\xi_2) - \left(\frac{\sqrt{\mu_1} - \sqrt{\mu_0}}{L}\right)\bar{g}_{ij}(r)\mu^{-1/2}(\xi_2) \quad (25)$$

where $\bar{f}_{ij}$ is $\hat{f}_{ij}$ without the shear modulus in the denominator and

$$\bar{g}_{ij} = \left[\begin{array}{c|c} \hat{g}_{21}n_1 + \hat{g}_{11}n_2 & \hat{g}_{22}n_1 + \hat{g}_{12}n_2 \\ \hat{g}_{11}n_1 + 3\hat{g}_{12}n_2 & \hat{g}_{12}n_1 + 3\hat{g}_{22}n_2 \end{array}\right]. \quad (26)$$

A rather interesting observation is that the second term in f_{ij}, which directly depends on fundamental solution g_{ij}, is non-symmetric as well (even for favorable values of the outward normal such as $\mathbf{n}=(1,0)$ or $\mathbf{n}=(0,1)$, which indicates that the direction of application of the point force is intertwined with the direction of the inhomogeneity in the Lamé parameter profiles.

4. The BEM solution

The BEM statement is formulated in the LT domain, where solution of the boundary-value problem is performed. A subsequent inverse Laplace transformation yields selective results (nodal displacements and/or tractions, element stresses) in the time domain. This is achieved numerically by employing Durbin's algorithm [41], whereby the transformed function of interest is sampled at discrete values of the transformed parameter as $s_k = 6.0/T + \mathrm{i}(2\pi/T)k,\ \ k = 0, 1, \ldots, N-1$, where N is the total number of points deemed necessary for an accurate inversion and given as $N = 2{\cdot}2{\cdot}5{\cdot}5\cdots$. Furthermore, T is the total time interval of interest and results are given at every time step $\Delta t = T/(N-1)$, starting with $t=0$. The aforementioned algorithm corresponds to numerical quadrature over the complex plane and it is known that the trailing part of the inverted function is not accurate (i.e., the last 10% of the time interval T).

The statement in the LT domain is based upon the usual reciprocity relation for the energy produced by the actual elastic state in the continuous body with volume V and surface S acting upon a reference (starred) elastic state [40]. Specifically,

$$\int \tilde{t}_i u_i^* \,\mathrm{d}S + \int \rho \tilde{f}_i u_i^* \,\mathrm{d}V = \int t_i^* \tilde{u}_i \,\mathrm{d}S + \int \rho f_i^* \tilde{u}_i \,\mathrm{d}V. \tag{27}$$

Since the starred state is identified with the fundamental solutions as $u_i^* = \tilde{g}_{ij}\mathbf{e}_j$ and $t_i^* = \tilde{f}_{ij}\mathbf{e}_j$ due to a point load $f_i^* = \delta(\mathbf{x}-\boldsymbol{\xi})e_i$, the final boundary integral equation when both $\mathbf{x}$, $\boldsymbol{\xi}$ are allowed on S is

$$c_{ij}(\boldsymbol{\xi})\tilde{u}_i(\boldsymbol{\xi}) = \int \tilde{g}_{ij}(\mathbf{x},\boldsymbol{\xi})\tilde{t}_j(\mathbf{x})\,\mathrm{d}S(\mathbf{x}) - \int \tilde{f}_{ij}(\mathbf{x},\boldsymbol{\xi})\tilde{u}_j(\mathbf{x})\,\mathrm{d}S(\mathbf{x}). \tag{28}$$

In the above, the jump term c_{ij} depends on the geometry at $\boldsymbol{\xi}$ in exactly the same fashion as for a homogeneous medium, because the singularity in the fundamental solutions has not changed. Also, one does not consider any body forces $\tilde{f}_i$ and the second integral is understood in the usual Cauchy principal-value sense. As shown in Fig. 1(b), the definition of the field $\boldsymbol{x}$ and receiver $\boldsymbol{\xi}$ points in the BEM statement is the reverse of that employed in the definition of the kernel functions.

Numerical solution of Eq. (28) follows along well-known lines, namely use of quadratic (three-noded) isoparametric surface elements along with a semi-analytical integration of the strong singularity exhibited by the traction kernel $\tilde{f}_{ij}$. More specifically, the static kernel is subtracted from the steady state kernel and the difference is integrated numerically using Gaussian quadrature. The singularity exhibited by the static kernel is found by the rigid-body motion concept. Since one is dealing with an inhomogeneous medium, it was necessary to derive the limiting form of $\tilde{f}_{ij}$ as $s\to 0$, which serves as the equivalent static kernel. For the weak singularity of the displacement kernel $\tilde{g}_{ij}$ one uses log-weighted Gaussian quadrature. If the singular node

Table 1
BEM program flowchart

(1)	Read input data: Determine mechanical properties, geometry, loading and boundary conditions, select *LT* parameter s_i range
(2)	*BEM* solution at each *LT* parameter value s_i: System matrix construction, solution of boundary-value problem, recovery of unknown boundary quantities, computation of stress components
(3)	*LT* inversion algorithm: Recover time-domain values of tractions/displacements/stresses that have been specified for inversion; for wave scattering problems, superimpose incident wave field
(4)	Write output data: Tables and plots

happens to be the middle one, then the corresponding element is further divided into two sub-elements on either side of the singularity.

Additional refinements [12] include viscoelastic material behavior, which is quite simple to implement in the LT domain through use of the correspondence principle, plus an infinite element derived from the quadratic one by allowing two nodes to move to infinity and employing appropriately modified shape functions. Finally, the matrix inversions required by the algebraic system of equations $[\tilde{\mathbf{G}}]\{\tilde{\mathbf{t}}\} = [\tilde{\mathbf{F}}]\{\tilde{\mathbf{u}}\}$ following imposition of the boundary conditions across the entire spectrum of s values is accomplished by Gaussian elimination, suitably modified to handle complex number formalism and non-symmetric system matrices. Table 1 is a summary of the BEM implementation. The aim here is to preserve a basic, modular-type BEM software platform in Fortran 90 where, through relatively simple changes in the specific modulus that contains the Green functions, it becomes possible to solve new classes of problems in elastodynamics.

5. Numerical examples

In this section, one uses the BEM to examine the dynamic behavior of underground circular cylindrical openings in an inhomogeneous 2-D continuum.

5.1. Wave speed profiles for the heterogeneous medium

The various constraints that appeared during the solution procedure for the Green functions in Sections 1 and 2 will now be examined in detail. At first, it was established that the elastic parameter profiles are quadratic functions of the depth co-ordinate $y = x_2$, as given by Eq. (8), and that $v = 0.25$. Constants *a, b* can be determined from values at two reference locations, namely $y = 0$ and L, which can be viewed as the depth co-ordinates of source and receiver points. Therefore, given that $\mu(0) = \mu_0$ and $\mu(L) = \mu_1$, one has

$$\lambda(y) = \mu(y) = ((\sqrt{\mu_1} - \sqrt{\mu_0})(y/L) + \sqrt{\mu_0})^2. \tag{29}$$

Furthermore, in order to employ Helmholtz's vector decomposition as discussed in Ref. [38], it was necessary to establish a density profile proportional to the elastic parameters. Thus, using Eq. (29) the result is

$$\rho(y) = \rho((\sqrt{\mu_1}/\sqrt{\mu_0} - 1)(y/L) + 1)^2. \tag{30}$$

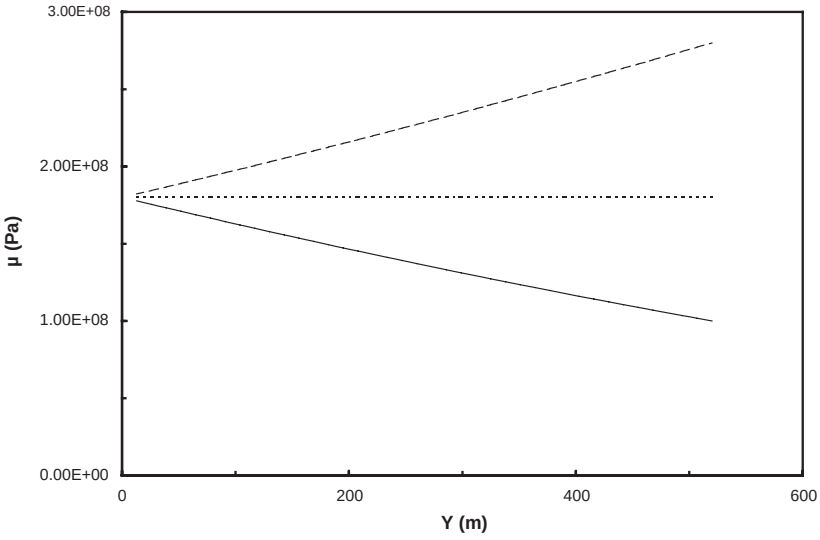

Fig. 2. Shear modulus variation with depth: ···, homogeneous; – – –, stiffening; ——, softening material.

The above material parameters yield wave speed profiles $c_1(y)$ and $c_2(y)$ that are macroscopically constant, i.e.,

$$c_1(y) = c_{10} = \sqrt{3\mu_0/\rho_0}, \qquad c_2(y) = c_{20} = \sqrt{\mu_0/\rho_0}. \tag{31}$$

In all the ensuing examples, one considers firm soil with 'background' material properties

$$\mu_0 = \lambda_0 = 180 \times 10^6 \text{ Pa}, \qquad \rho_0 = 2000\,\text{kg/m}^3,$$
$$c_{10} = 519.6\,\text{m/s}, \qquad c_{20} = 300.0\,\text{m/s}. \tag{32}$$

Two basic shear modulus profiles will be examined, namely one where the material stiffens with increasing depth and another where it becomes softer. Specifically, $\mu_1 = 280 \times 10^6$ Pa in the former case and $\mu_1 = 100 \times 10^6$ Pa in the latter case. The length scale over which this variation takes place is $L = 520$ m, which coincides with the wavelength of the P-wave at a vibration frequency of $f = 1.0$ Hz. Both these profiles are shown in Fig. 2.

Next, Figs. 3 and 4, respectively, plot the non-zero components of the displacement and traction fundamental solutions (Eqs. (16) and (25), respectively) that register along a vertical line from the source at $y = 0$ where unit point forces are applied downwards to $y = L$, i.e., along the direction of the inhomogeneity. As expected, the displacements increase and the tractions decrease in the stiffening material as the receiver moves downwards. The opposite trend is observed for the softening material.

5.2. Comparison study

One first examines a circular cylindrical cavity of radius $r = a = 0.381$ m in the "background" homogeneous medium described above, as it is being engulfed by a *P*-wave propagating from a

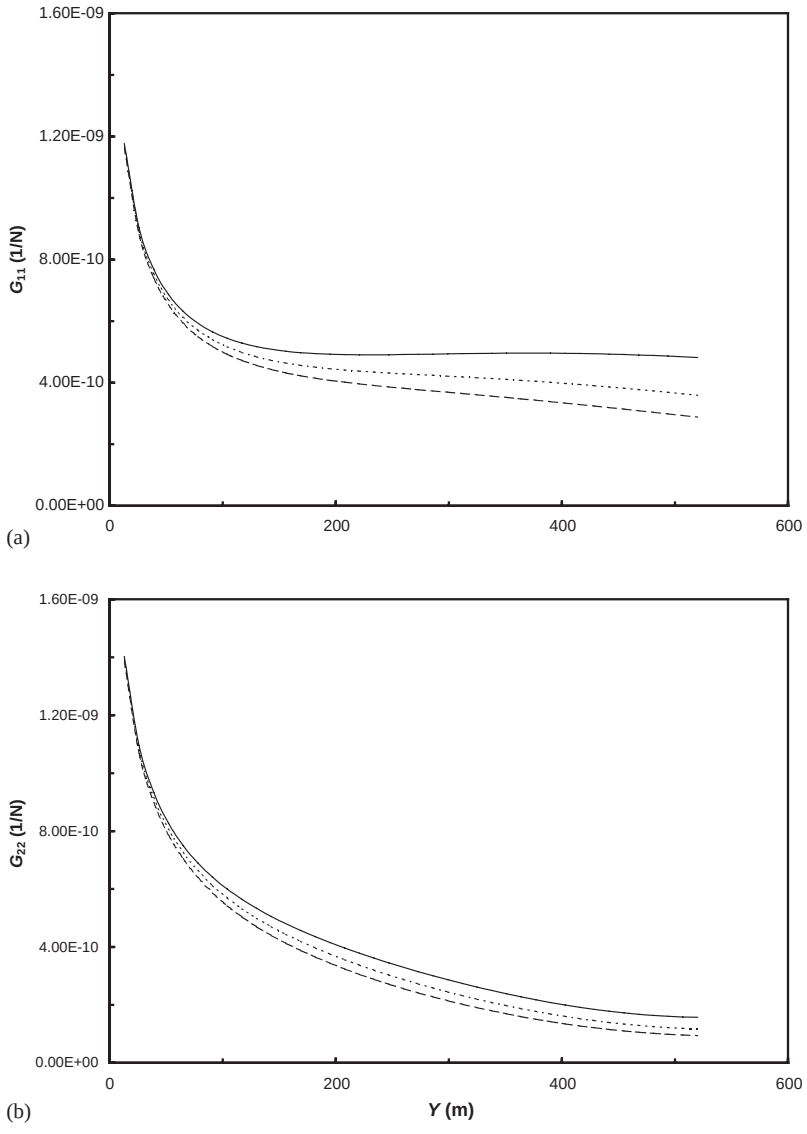

Fig. 3. Displacement fundamental solution component of (a) G_{11} and (b) G_{22} at $f = 1.0$ Hz: ···, homogeneous; – – –, stiffening; ——, softening material.

point source at infinity. Behind the wave front, the following incident stress field develops as

$$\sigma^i_{xx} = \sigma_0, \qquad \sigma^i_{yy} = (v/(1-v))\sigma_0 = \varepsilon\sigma_0, \qquad \sigma^i_{xy} = 0, \tag{33}$$

where σ_0 is taken as 10^5 Pa and $\varepsilon = \frac{1}{3}$ for the Poisson ratio of 0.25. At the same time, the radial and tangential components of the incident displacement field are

$$u^i_r = -(\sigma_0/rc_1)\cos\theta[t - t^*], \qquad u^i_\theta = -(\sigma_0/rc_1)\sin\theta[t - t^*] \tag{34}$$

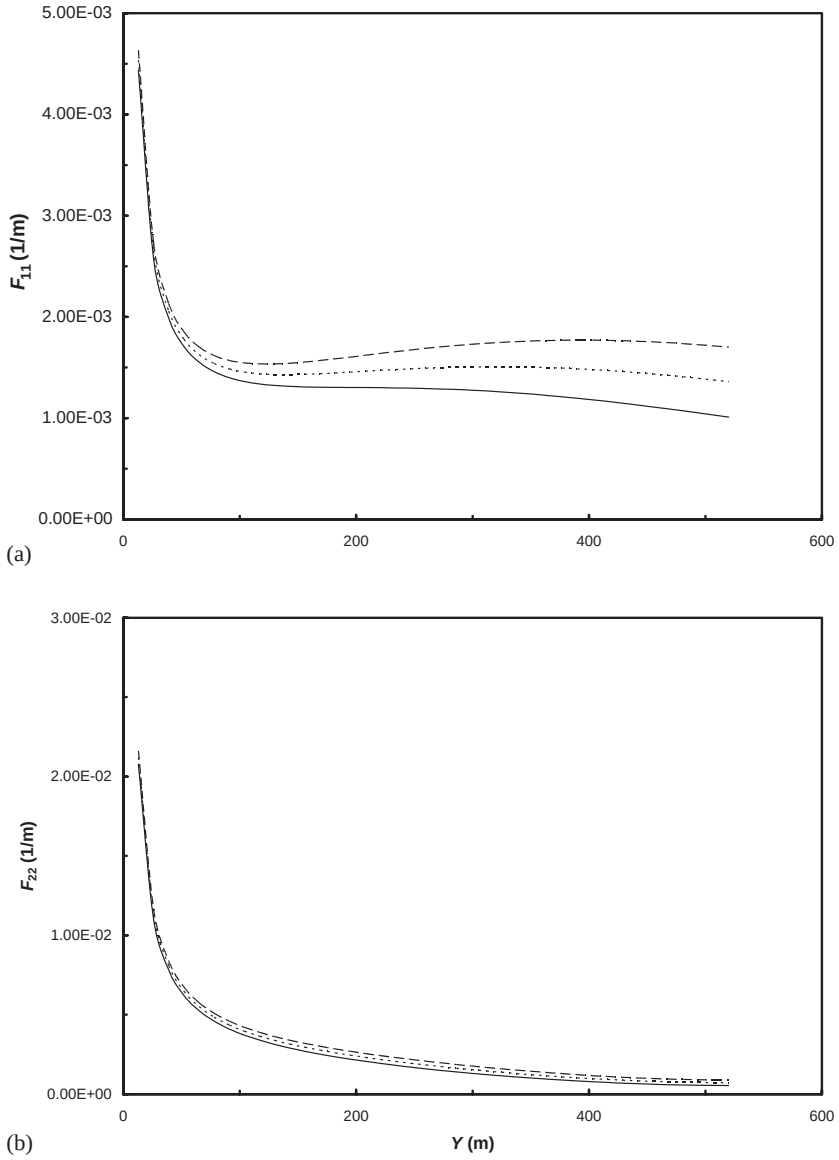

Fig. 4. Traction fundamental solution components of (a) F_{11} and (b) F_{22} at $f = 1.0$ Hz: $\cdots$, homogeneous; – – –, stiffening; ——, softening material.

and delay t^* is the time required for the wave to reach a particular station (a, θ) on the cavity's perimeter, i.e.,

$$t^* = a(1 - \cos\theta)/c_1. \tag{35}$$

Obviously, $t^* = 0$ at the point of first impact, which would be station 1 at $\theta = 0$ in Fig. 5(a) for an angle of incidence $\varphi = 0^\circ$. One notes here that the total field is understood to be the sum of incident

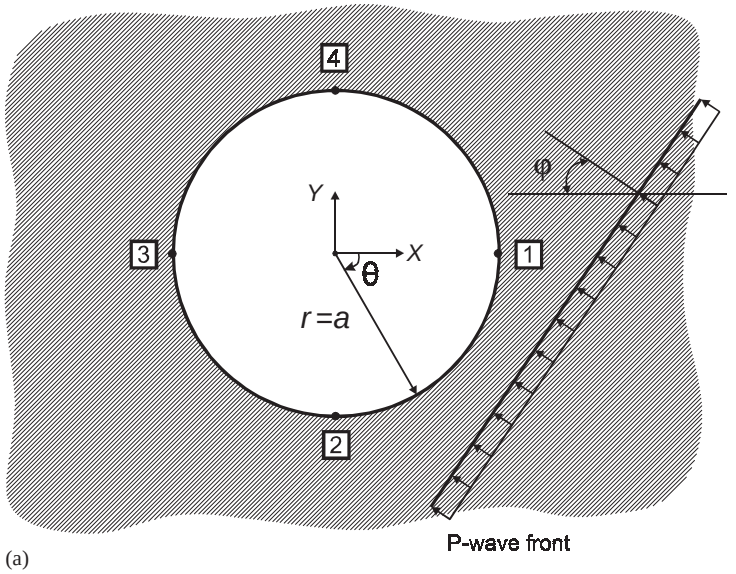

(a)

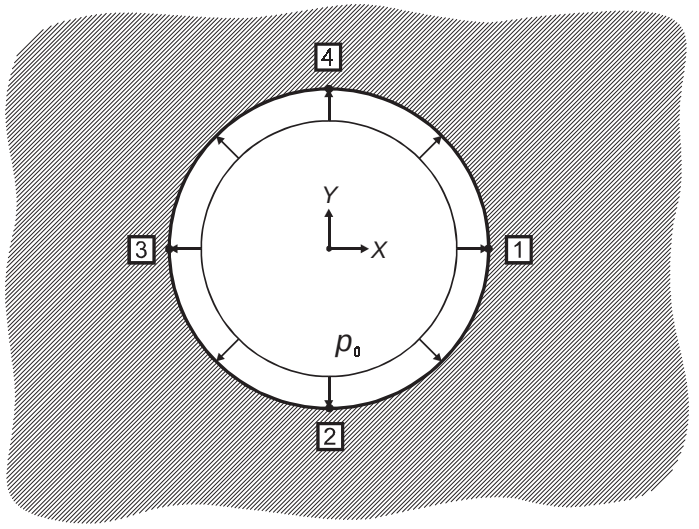

(b)

Fig. 5. Circular cylindrical cavity under (a) pressure wave sweep with arbitrary angle of incidence φ and (b) sudden internal pressure.

(*i*) plus scattered (*s*) fields; in the case of displacements, a rigid-body motion component can be extracted as the cavity displaces in the direction of the incoming wave. Finally, an intrinsic time scale can be computed for this material as the time require for the *P*-wave to traverse distance *2a*, i.e.,

$$t_0 = 2a/c_1 = 0.001467\,\text{s}. \tag{36}$$

An analytical solution for the total stress produced around the cavity wall during and after wave passage appears in Baron and Matthews [42]. Specifically, an integral transform technique is employed and the ensuing expressions for the radial (σ_{rr}) and hoop ($\sigma_{\theta\theta}$) stresses are derived in the time domain following analytical inversion over the complex frequency plane. The results are normalized by dividing with the incident stresses and are plotted as stress concentration factors $SCF = (\sigma^s_{\theta\theta} + \sigma^i_{\theta\theta})/\sigma^i_{\theta\theta}$ versus dimensionless time $T = c_1 t/2a$. The same basic approach was subsequently used by Baron and Parnes [43] for the cavity wall displacement field normalized as $U^s_i = u^s_i \mu/(\sigma_0 a)$ versus T. Finally, the analytical results are inaccurate at early times, up to about one full transit time t_0, because of the limited number of terms retained in the series expansion of the relevant fields in the transformed domain. It is mentioned in the aforementioned references that a short-time asymptotic solution would be necessary for very early times, limited to the illuminated zone of the cavity, i.e., the region $|\theta| < 60^\circ$.

One imposes the following boundary-value problem on the BEM formulation of Section 4

$$t_x = \sigma^i_{xx} \cos\theta + \sigma^i_{xy} \sin\theta, \qquad t_y = \sigma^i_{xy} \sin\theta + \sigma^i_{yy} \cos\theta. \tag{37}$$

One then solves for the displacement field (u_x, u_y), from which the stress field (σ_{xx}, σ_{yy}, σ_{xy}) can be derived by combining the last two of Eqs. (1), introducing derivatives of the strains in the normal (n) tangential (q) directions as $\partial u_i/\partial n = (\partial u_i/\partial x_i)(\partial x_i/\partial n)$, $\partial u_i/\partial q = (\partial u_i/\partial x_i)(\partial x_i/\partial q)$ and using finite differences. This solution corresponds to the scattered field. All BEM results have been normalized as previously mentioned and are plotted in Figs. 6 and 7. One observes a reasonably good agreement between analytical and BEM results, especially past the first full transit time interval t_0 (or $T = 1$). The BEM solution is stable in the sense that any space discretization past 16 elements and any LT parameter sampling of over 20 points yields the same results at comparable locations and time instants. Furthermore, the results reproduce the jump associated with wave signal arrival and smoothly decay to the values predicted by the static solution [44]. The maximum dynamic SCF is 2.9 and appears at the top and bottom stations.

5.3. Cavity under sudden explosion

The next series of results pertains to the circular cylindrical cavity of radius α under sudden radial pressure $p_0 = 10^5$ Pa applied (and maintained) at the cavity walls. One assumes that the cavity is at a certain depth from the free surface of a half-plane, so that no reflected or surface waves are present. The BEM solution is obtained by imposing tractions along the boundary. As mentioned in the previous sub-section, the basic discretization schemes are either 16 elements yielding 32 nodal points or 32 elements yielding 64 nodal points. Furthermore, either 20 or 50 LT sampling points are used with each spatial discretization scheme. The results shown below are for the 16 element and 50 LT point combination.

Cavity expansion in a homogeneous medium is a problem with radial symmetry. In the presence of inhomogeneity, this is no longer true and it becomes necessary to compute the radial displacement u_r and the hoop stress $\sigma_{\theta\theta}$ at three (at least) representative locations on the perimeter, namely stations 1, 2 and 4 that are shown in Fig. 5(b). One notes here that reference length L is set equal to the cavity diameter, while the relative orientation of the cavity itself is such that $\mu = \mu_0$ is associated with the top station (no. 4 at $\theta = 270^\circ$) and $\mu = \mu_1$ with the bottom station (no. 2 at $\theta = 90^\circ$). Figs. 8 and 9, respectively, plot the time variations of u_r and $\sigma_{\theta\theta}$ and contrast

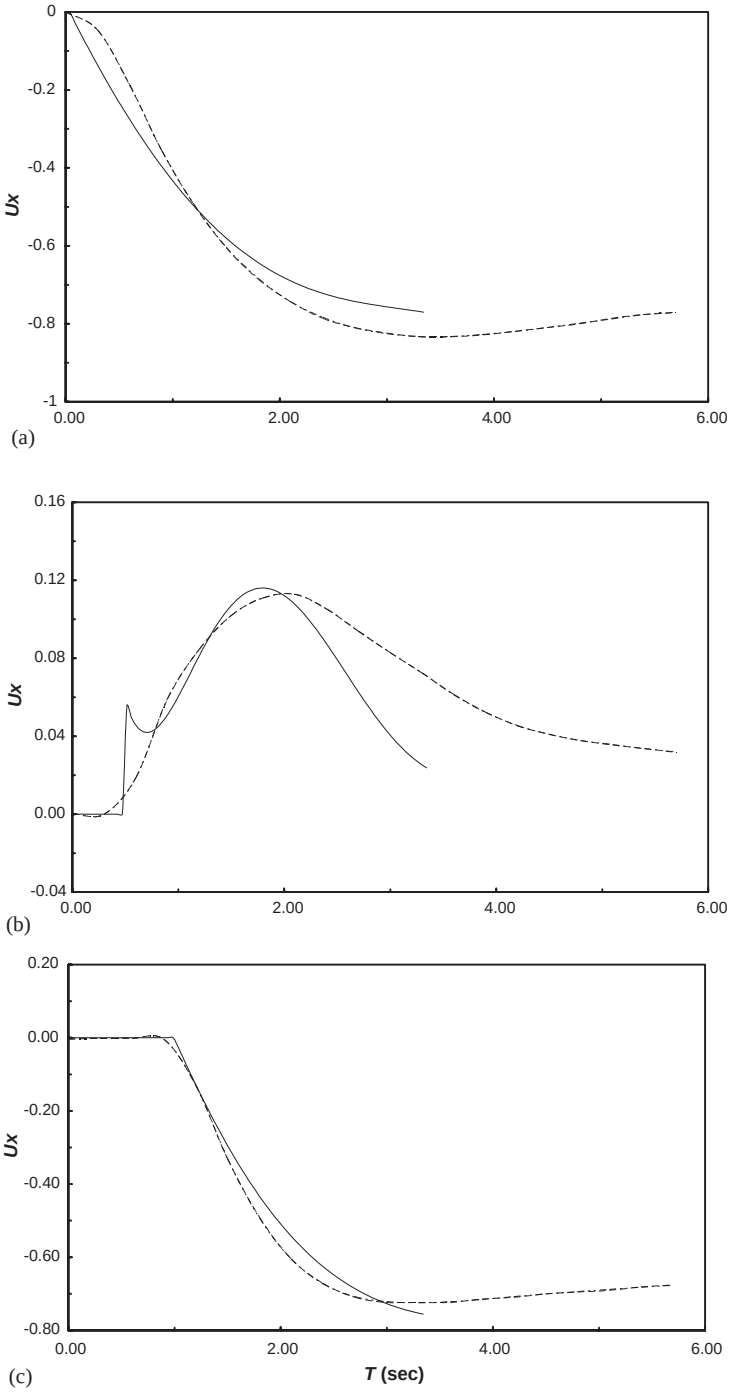

Fig. 6. Comparison of scattered normalized displacements in a cavity buried in a homogeneous continuum under a *P*-wave: (a) station 1 at $\theta = 0^\circ$, (b) station 2 at $\theta = 90^\circ$ and (c) station 3 at $\theta = 180^\circ$. -·· -, 16 BE, 20 LT pts; – – –, 32 BE, 20 LT pts; ——, analytical solution.

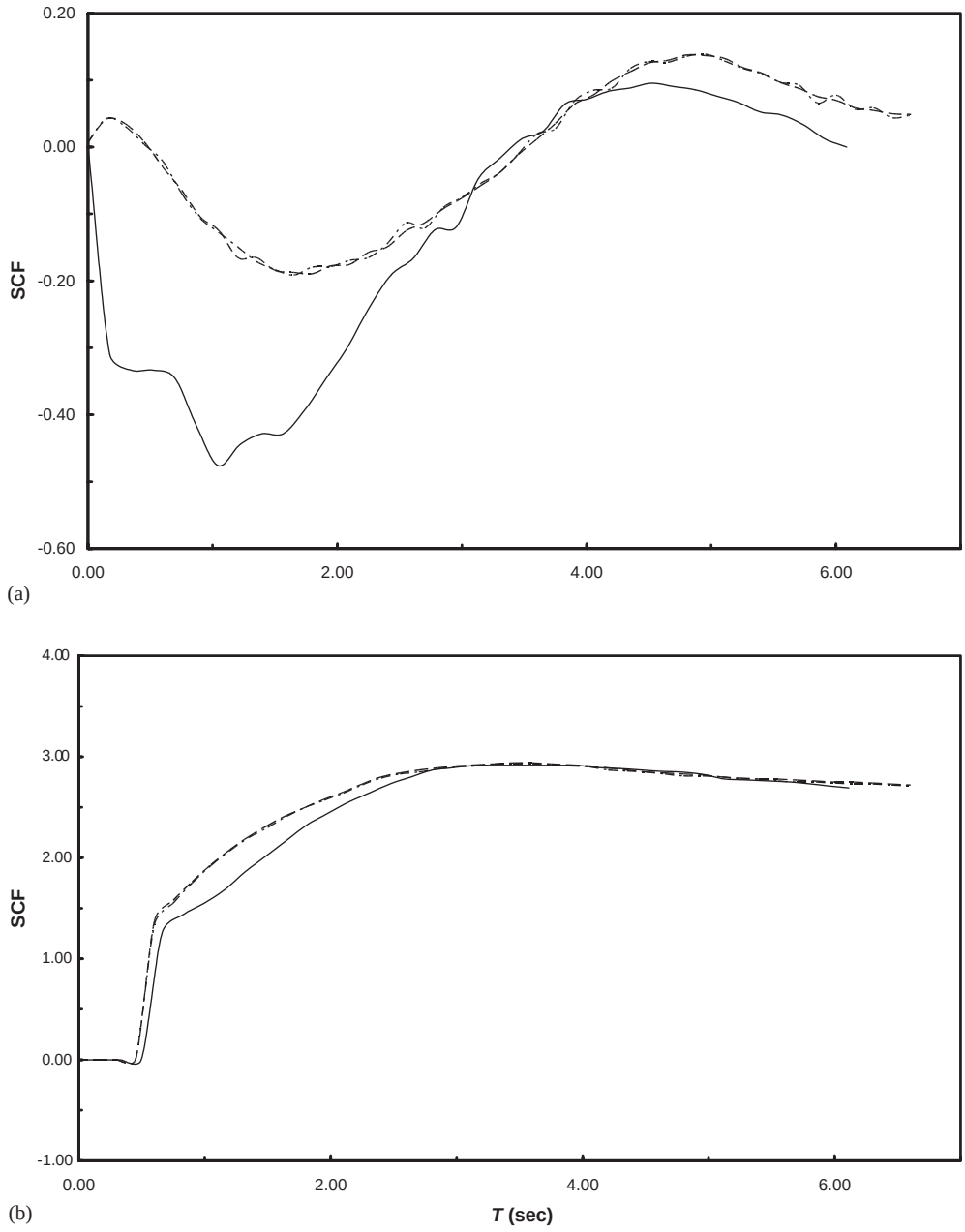

Fig. 7. Comparison of stress concentration factors in a cavity buried in a homogeneous continuum under a *P*-wave: (a) station 1 at $\theta = 0^\circ$ and (b) station 2 at $\theta = 90^\circ$. -· ··-, 16 BE, 20 LT pts; – – –, 32 BE, 20 LT pts; ——, analytical solution.

them with the solution obtained for a homogeneous background ($\mu = \mu_0$). One observes that the radial motion at the equator is virtually unaffected by variations in the shear modulus; at the top station, however, a very different picture emerges in that the crown sinks in. At the bottom,

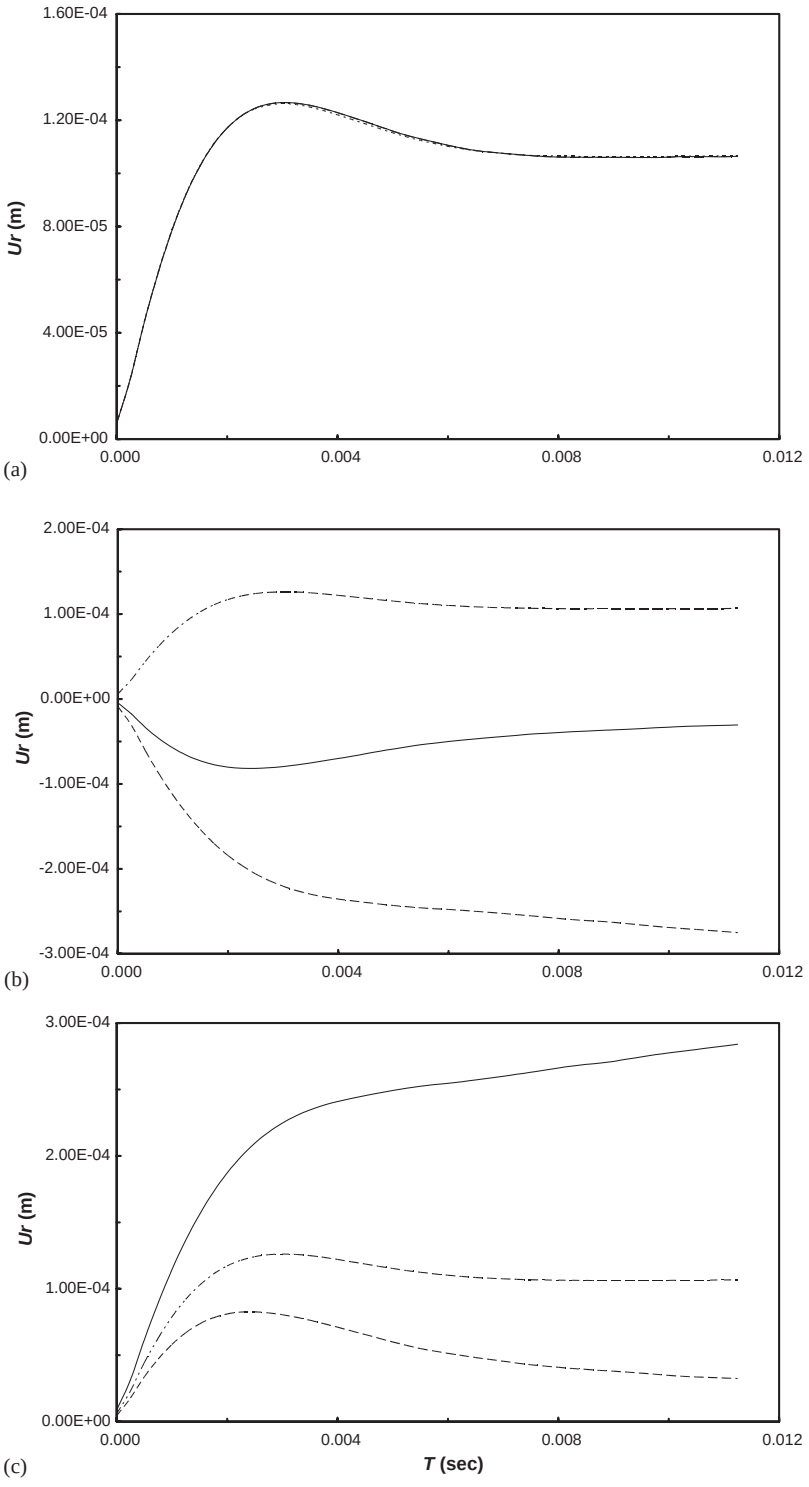

Fig. 8. Displacement time history due to internal explosion: (a) station 1 at $\theta = 0^\circ$, (b) station 2 at $\theta = 90^\circ$ and (c) station 4 at $\theta = 270^\circ$. ⋯, homogeneous; – – –, stiffening; ——, softening material.

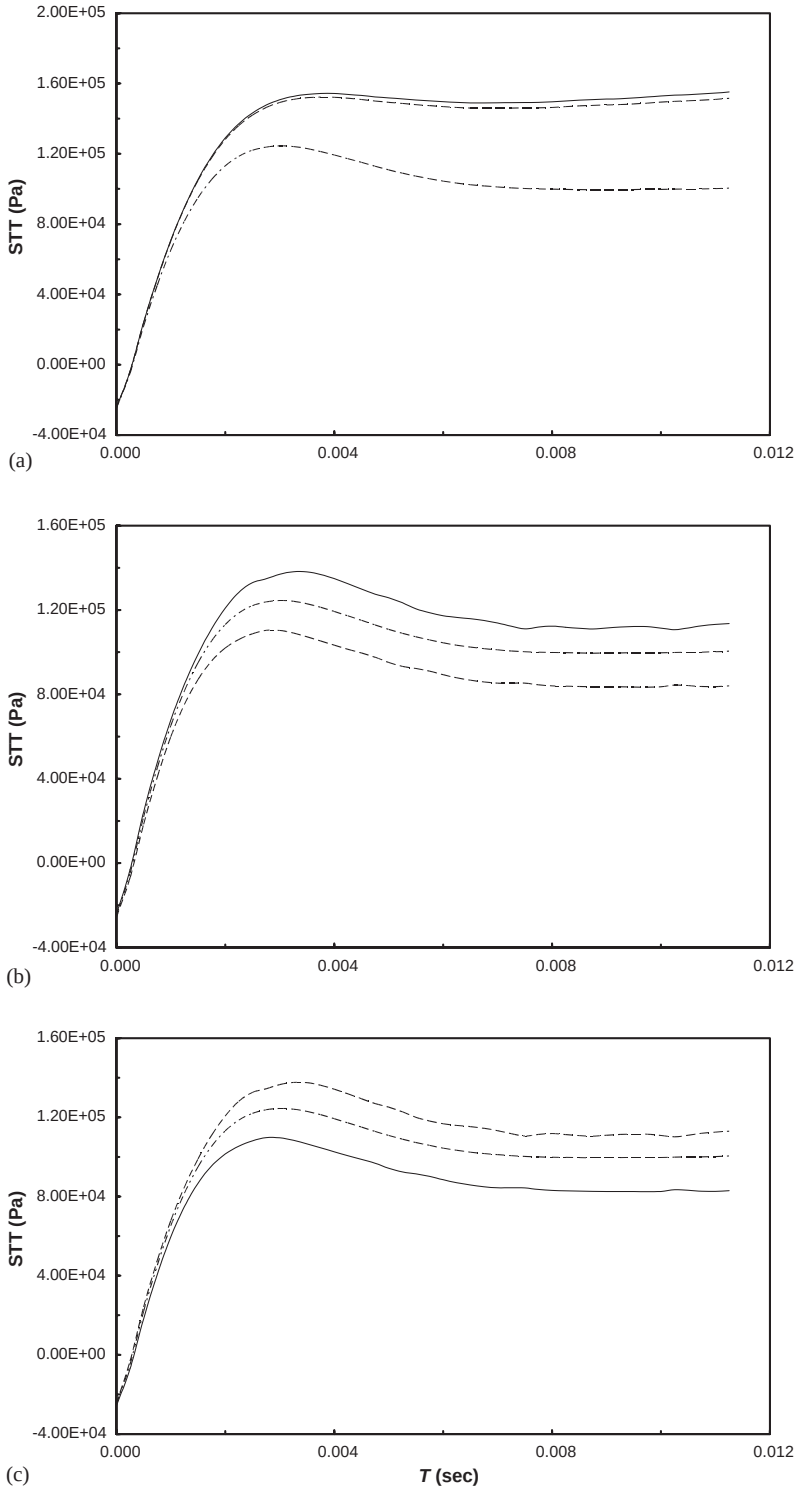

Fig. 9. Hoop stress time history due to internal explosion: (a) station 1 at $\theta = 0^\circ$, (b) station 2 at $\theta = 90^\circ$ and (c) station 4 at $\theta = 270^\circ$. ⋯, homogeneous; – – –, stiffening; ——, softening material.

displacements show outward movement and are higher for the softer material and lower for the stiffer material, as compared to the homogeneous background solution. Essentially, the cavity no longer expands uniformly but assumes a distorted oval shape that depends on whether the material is becoming softer or stiffer. As far as the transient hoop stresses at the equator are concerned, there is little difference between the stiffer and softer materials, but both overshoot the homogeneous material solution. Finally, at both top and bottom stations, the inhomogeneous material stresses bracket the homogenous stresses. The SCF here is simply the ratio $\sigma_{\theta\theta}/p_0$. Given the normalized value for p_0, the highest SCF observed are 1.56 at the equator and 1.38 at the poles, versus 1.25 that would uniformly valid for the homogeneous material.

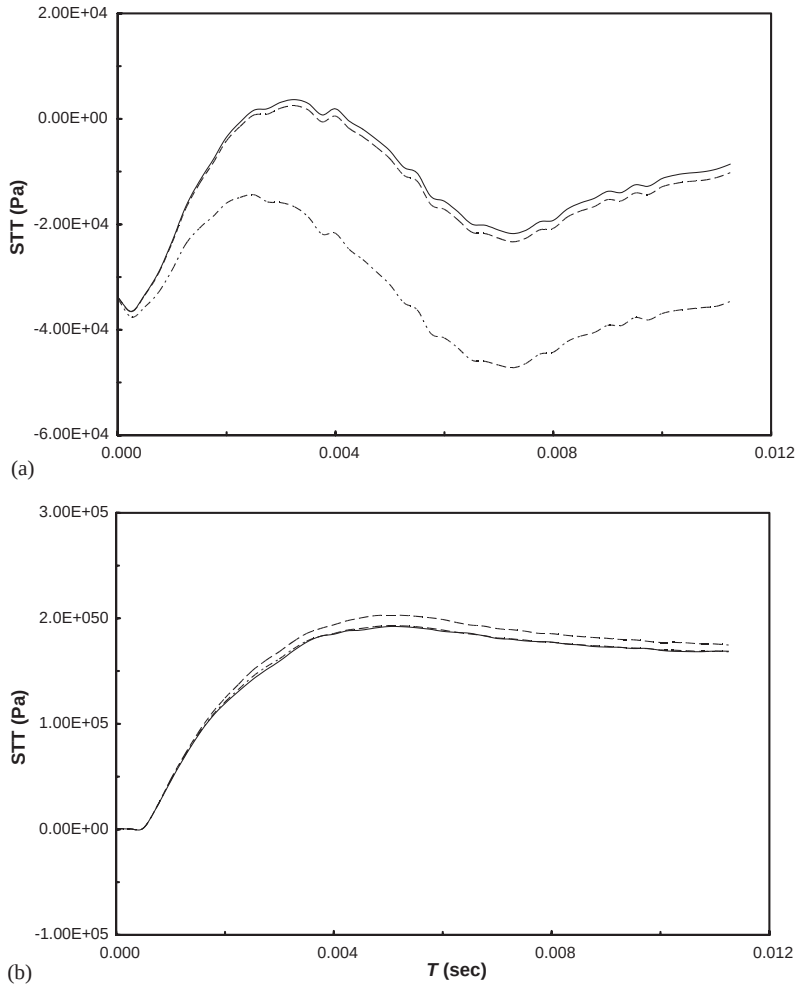

Fig. 10. Hoop stress time history due to *P*-wave sweep impinging at $\varphi = 0°$: (a) station 1 at $\theta = 0°$, (b) station 2 at $\theta = 90°$, (c) station 3 at $\theta = 180°$ and (d) station 4 at $\theta = 270°$. $\cdots$, homogeneous; – – –, stiffening; ——, softening material.

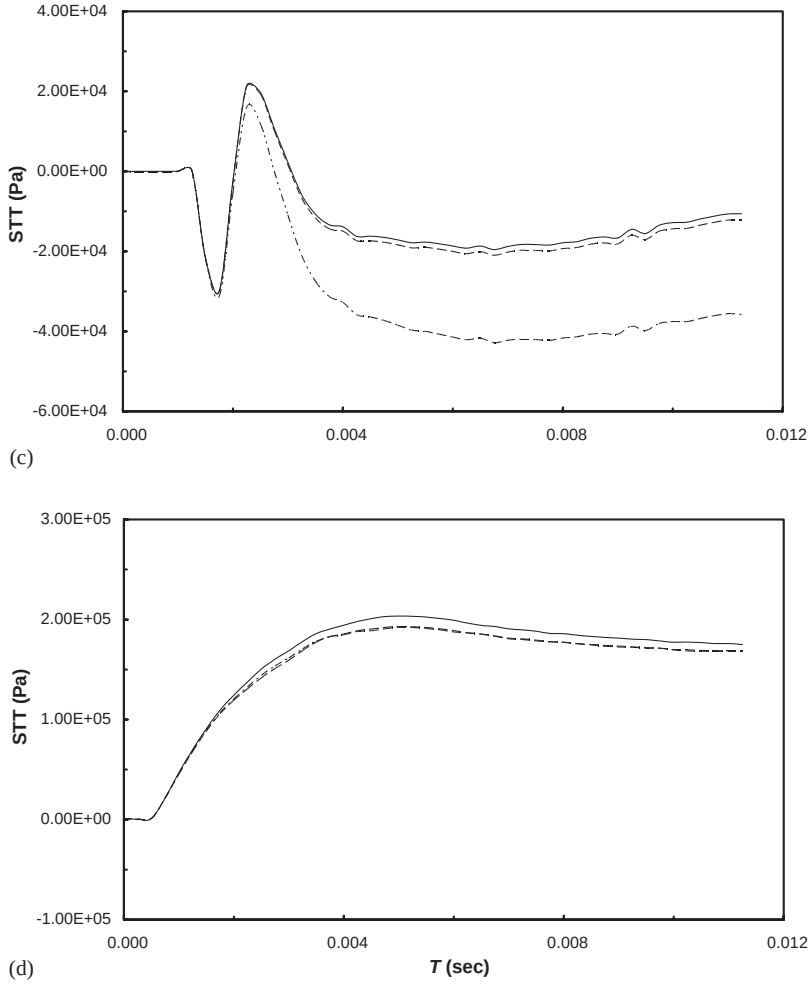

Fig. 10 (*continued*).

5.4. Cavity under pressure wave sweep

This is essentially the same problem solved in the comparison study, except that two additional parameters enter the analysis: (a) The increase or decrease in the shear modulus registered in the vertical direction and along a reference distance of $L=2a$, and (b) the direction of the incoming P-wave measured with respect to angle φ between the normal to the wave front and the x-axis. Since the incident field is known and was given in Section 5.2, all results in Figs. 10 (horizontally travelling wave) and 11 (vertically travelling wave) pertain to scattered hoop stress so as to facilitate the comparison between inhomogeneous and homogenous media. Also, the dynamic SCF can always be reconstituted by using first principles.

As the P-wave sweeps the cavity along the horizontal direction, the critical stress state is that developing at the top and bottom stations. For the stiffer profile, there is an overshoot of about 10% at the bottom and no measurable difference at the top as compared to the homogeneous

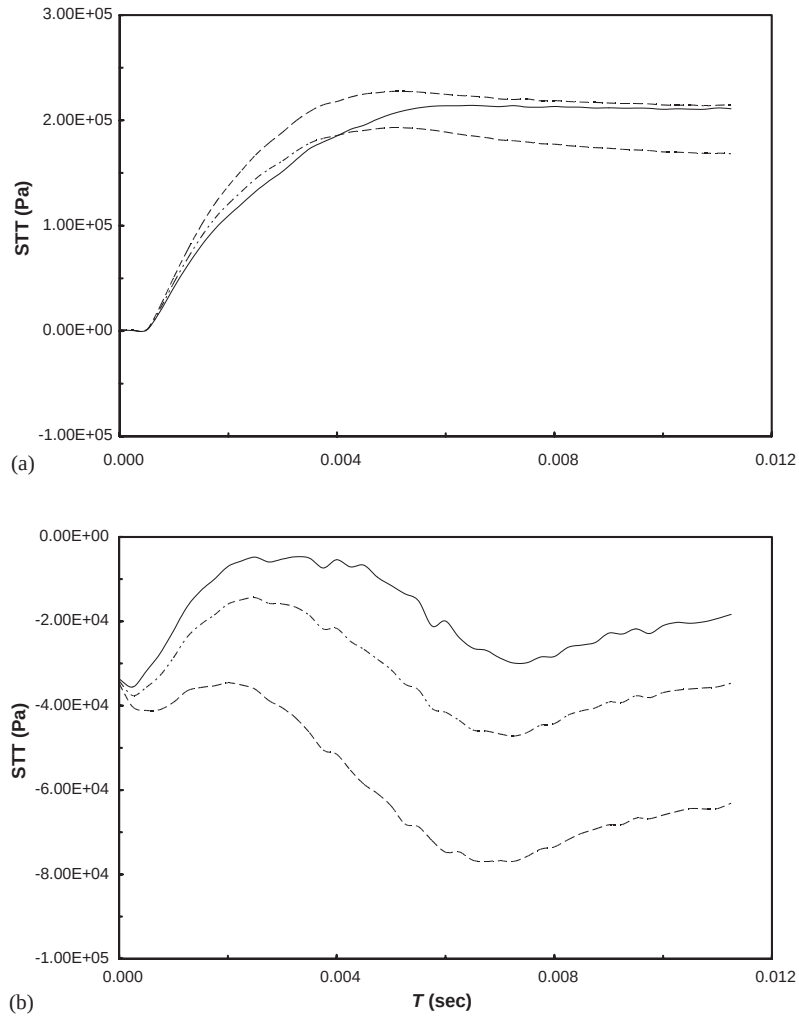

Fig. 11. Hoop stress time history due to *P*-wave sweep impinging at $\varphi = 90^\circ$: (a) Station 1 at $\theta = 0^\circ$, (b) station 2 at $\theta = 90^\circ$, (c) station 3 at $\theta = 180^\circ$ and (d) station 4 at $\theta = 270^\circ$. ⋯, homogeneous; – – –, stiffening; ——, softening material.

material. The reverse situation is observed for the softer profile. One notes here that the scattered hoop stresses overshoot the incident stress by a factor of 1.9 in the homogeneous material, which is precisely what produces the SCF of 2.9 discussed in the comparison study. The hoop stresses at stations 1 and 3 along the equator are of minor importance and, in fact, are an order of magnitude less than the stresses at stations 2 and 4. One observes that after an early time interval, the inhomogeneous material stresses diverge from those in the homogeneous background and, for the most part, are smaller in absolute value terms.

The final case has to do with the *P*-wave sweeping the cavity from below and in the direction of the varying shear modulus profile. The key locations are now the two stations along the equator. There, the hoop stresses overshoot the homogeneous material solution by factors of about 20%

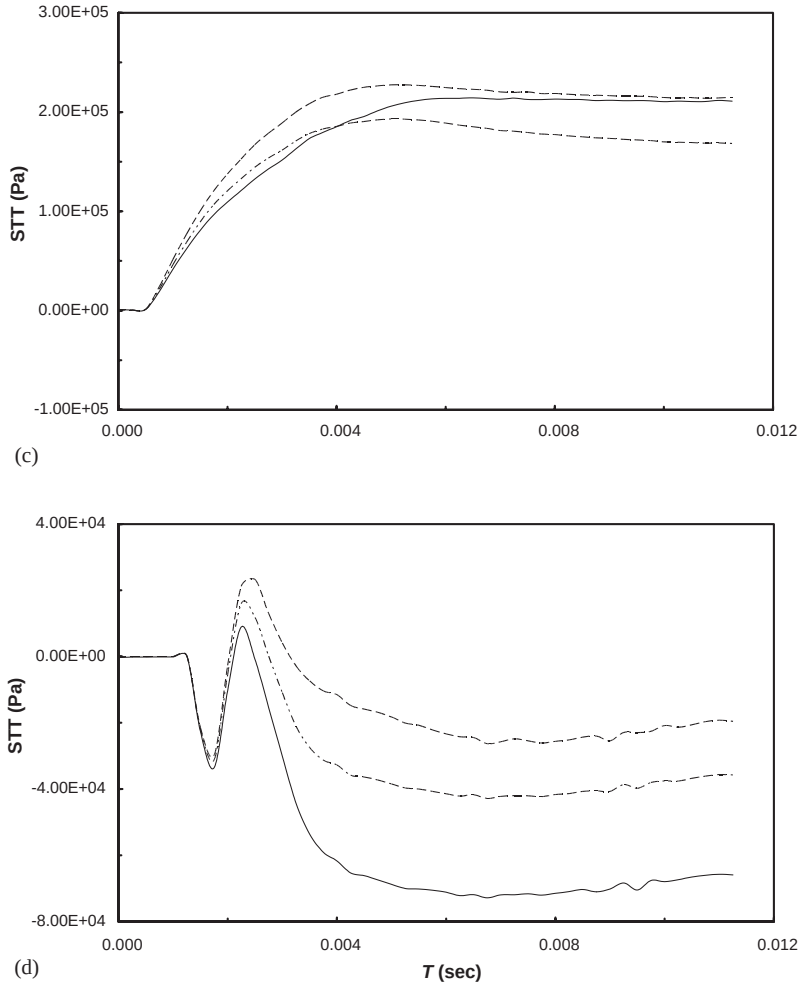

Fig. 11 (*continued*).

and 15% for the stiffening and softening material, respectively. The difference is that the rise in the stress is more rapid for the former type of inhomogeneity. As far as the stresses at the point of first impact and its counterpart in the shadow zone are concerned, one sees that they act as bounds for the homogeneous hoop stress. In absolute value terms, the larger stress registered at Station 2 in the illuminated zone is that for the stiffening material; the reverse holds true at Station 4.

6. Conclusions

In this work, a BEM has been developed for the solution of wave scattering problems in buried cavities by using the appropriate Green's function that obviate the need for any interior discretization. Specifically, these functions are derived by combining algebraic transformations of

the displacement vector with Helmholtz's decomposition in a restricted class of 2-D heterogeneous continua and under time-harmonic conditions. This type of solution is for a point impulse in the continuum and is subjected to certain constraints that arise during the course of the solution procedure. Specifically, the constraints correspond to elastic modulii that have a quadratic variation with respect to the depth co-ordinate, the Poisson ratio of 0.25 and a density profile proportional to that of the shear modulus. BEM implementation is straightforward and requires a rather modest discretization effort for this class of problems. For simple cases such as signal transmission along the vertical direction, the results (given directly by the Green functions) are predictable: if the material stiffens with depth, displacements decrease and forces increase in that direction. When boundary-value problems involving openings in the inhomogeneous continuum are solved, however, the picture that emerges is far more complex. This is due to the interplay between geometry and material inhomogeneity and furthermore depends on the type and direction of the loading. Invariable, larger dynamic stress concentration factors are recovered along the cavity perimeter for the inhomogeneous medium as compared to the homogeneous background case.

References

[1] W.M. Ewing, W.S. Jardetzky, F. Press, Elastic Waves in Layered Media, McGraw-Hill, New York, 1957.
[2] J.D. Achenbach, Wave Propagation in Elastic Solids, North-Holland, Amsterdam, 1973.
[3] K.F. Graff, Wave Motion in Elastic Solids, University of Ohio Press, Columbus, OH, 1973.
[4] L.M. Brekhovskikh, O.A. Godin, Acoustics of Layered Media II: Point Sources and Bounded Beams, Springer, Berlin, 1992.
[5] K. Helbig, Modeling the Earth for Oil Exploration, Pergamon/Elsevier Science, Oxford, 1994.
[6] A.H. Nayfeh, Wave Propagation in Layered Anisotropic Media with Applications to Composites, North-Holland, Amsterdam, 1995.
[7] V.K. Kinra, B.K. Henderson, K.I. Maslov, Elastodynamic response of layers of spherical particles in hexagonal and square periodic arrangements, Journal of the Mechanics and Physics of Solids 47 (1999) 2147–2170.
[8] R.P. Shaw, P. Bugl, Transmission of plane waves through layered linear viscoelastic media, Journal of the Acoustical Society of America 46 (1969) 649–654.
[9] S. Torquato, Random heterogeneous media: Microstructure and improved bounds on effective properties, Applied Mechanics Reviews 44 (1991) 37–76.
[10] P.S. Dineva, G.D. Manolis, Scattering of seismic waves by cracks in multi-layered geological regions I. Mechanical model & II. Numerical results, Soil Dynamics and Earthquake Engineering 21 (2001) 615–625 and 627–641.
[11] J.F. Allard, Propagation of Sound in Porous Media: Modeling Sound Absorbing Materials, Elsevier Applied Science, London, 1993.
[12] G.D. Manolis, D.E. Beskos, Boundary Element Methods in Elastodynamics, Chapman & Hall, London, 1988.
[13] J. Dominguez, Boundary Elements in Dynamics, Computational Mechanics Publications, Southampton, 1993.
[14] L.M. Brekhovskikh, R. Beyer, Waves in Layered Media, 2nd Edition, Academic Press, Cambridge, 1976.
[15] W.E. Chew, Waves and Fields in Inhomogeneous Media, Van Nostrand-Reinhold, New York, 1990.
[16] O. Nishizawa, T. Satoh, X. Lei, Y. Kuwahara, Laboratory studies of seismic wave propagation in inhomogeneous media using a laser Doppler vibrometer, Bulletin of the Seismological Society of America 87 (1997) 804–823.
[17] E. Kausel, G. Manolis, Wave Motion in Earthquake Engineering, WIT Press, Southampton, 2000.
[18] R.J. Geller, T. Ohminato, Computation of synthetic seismograms and their partial derivatives for heterogeneous media with arbitrary natural conditions using the Direct Solution Method, Geophysics Journal International 116 (1994) 421–446.

[19] P. Moczo, E. Bystricky, J. Kristek, J.M. Carcione, M. Bouchon, Hybrid modeling of P-SV seismic motion at inhomogeneous viscoelastic topographic structures, Bulletin of the Seismological Society of America 87 (1997) 1305–1323.
[20] S.M. Kim, S.T. Liao, J.M. Roesset, Simulation of the cross-hole method in isotropic and anisotropic media, International Journal for Numerical and Analytical Method in Geomechanics 23 (1999) 1101–1119.
[21] R.F. Gragg, One-way propagation in weakly nonuniform media, Wave Motion 27 (1998) 95–115.
[22] G. Muravskii, Parameters determination for a linearly inhomogeneous half-space using characteristics of the time-harmonic surface waves, Earthquake Engineering and Structural Dynamics 29 (2000) 399–418.
[23] V.V. Volovoi, D.H. Hodges, V.L. Berdichevsky, V.G. Sutyrin, Dynamic dispersion curves for non-homogeneous, anisotropic beams with cross-sections of arbitrary geometry, Journal of Sound and Vibration 215 (1998) 1101–1120.
[24] G.D. Manolis, Stochastic soil dynamics, Soil Dynamics and Earthquake Engineering 23 (2002) 3–15.
[25] S. Hazanov, On apparent properties of nonlinear heterogeneous bodies smaller than the representative volume, Acta Mechanica 134 (1999) 123–134.
[26] D.E. Beskos, Boundary element methods in dynamic analysis, Applied Mechanics Reviews 40 (1987) 1–23.
[27] D.E. Beskos, Boundary element methods in dynamic analysis: part II, 1986–1996, Applied Mechanics Reviews 50 (1997) 149–197.
[28] Y.A. Melnikov, Green's Functions in Applied Mechanics, Computational Mechanics Publications, Southampton, 1995.
[29] P.W. Partridge, C.A. Brebbia, L.C. Wrobel, The Dual Reciprocity Boundary Element Method, Computational Mechanics Publications, Southampton, 1992.
[30] L. Chen, A.J. Kassab, D.W. Nicholson, M.B. Chopra, Generalized boundary element method for solids exhibiting non homogeneities, Engineering Analysis with Boundary Elements 25 (2001) 407–422.
[31] M. Itagaki, Advanced dual-reciprocity method based on polynomial source and its application to eigenvalue problem for non uniform media, Engineering Analysis with Boundary Elements 24 (2000) 169–176.
[32] S.Q. Xu, N. Kamiya, A formulation and solution for boundary element analysis of inhomogeneous nonlinear problem, Computational Mechanics 22 (1998) 367–374.
[33] A. Tadeu, J. Antonio, 2.5 Green's functions for elastodynamic problems in layered acoustic and elastic formations, Computer Methods in Engineering Science 2 (2001) 477–496.
[34] W. Wang, H. Ishikawa, A method for linear elastostatic analysis of multi-layered axisymmetric bodies using Hankel's transform, Computational Mechanics 27 (2001) 474–483.
[35] M.I. Azis, D.L. Clements, A boundary element method for anisotropic inhomogeneous elasticity, International Journal of Solids and Structures 38 (2001) 5747–5763.
[36] B.B. Guzina, R.Y.S. Pak, Elastodynamic Green's functions for a smoothly heterogeneous half-space, International Journal of Solids and Structures 33 (1996) 1005–1021.
[37] C. Vrettos, The Boussinesq problem for soils with bounded non-homogeneity, International Journal for Numerical and Analytical Method in Geomechanics 22 (1998) 655–669.
[38] G.D. Manolis, R.P. Shaw, Green's function for the vector wave equation in a mildly heterogeneous continuum, Wave Motion 24 (1996) 59–83.
[39] A.I. Zayed, Handbook of Function and Generalized Function Transforms, CRC Press, Boca Raton, FL, 1996.
[40] T.A. Cruse, F.J. Rizzo, A direct formulation and numerical solution for the general transient elastodynamic problem—I, Journal of Mathematical Analysis and Applications 22 (1968) 244–259.
[41] F. Durbin, Numerical inversion of Laplace transforms: an efficient improvement to Dubner and Abate's method, Computation Journal 17 (1974) 371–376.
[42] M.L. Baron, A.T. Matthews, Diffraction of a pressure wave by a cylindrical cavity in an elastic medium, Journal of Applied Mechanics 28 (1961) 347–354.
[43] M.L. Baron, R. Parnes, Displacements and velocities produced by the diffraction of a pressure wave by a cylindrical cavity in an elastic medium, Journal of Applied Mechanics 29 (1962) 385–395.
[44] G.N. Savin, Stress Concentration Around Holes, Pergamon Press, New York, 1961.